Local spin susceptibility in the zero-gap-semiconductor state of α-(BEDT-TTF)$_2$I$_3$ probed by ^{13}C NMR under pressure

Shinji Hirose and Atsushi Kawamoto*
Department of Condensed Matter Physics, Hokkaido University, Kita-ku, Sapporo, Hokkaido 060-0810, Japan
(Received 11 June 2010; revised manuscript received 28 July 2010; published 16 September 2010)

α-(BEDT-TTF)$_2$I$_3$ has a double column structure with three crystallographically independent molecules, A, B, and C, and becomes an insulator below 135 K due to a charge-ordering (CO) transition. The CO state is suppressed under pressure and shows weak temperature dependence of the electrical resistance. The decline of the carrier density is observed over 1.8 GPa, suggesting a zero-gap-semiconductor state under high pressure. The local susceptibility on each site provides important information about the electronic band structure. In our previous work, molecular site B became spin poor and molecular site C became spin rich in the metallic state, suggesting the disproportionation of the local spin density. Therefore, it is worthwhile to investigate the behavior of the electron properties of each molecular site. We accessed the ^{13}C-NMR in this salt at ambient pressure and at 2.1 GPa. The analysis of the local spin susceptibility suggests that the disproportionation of the spin susceptibility at 2.1 GPa is enhanced from that at ambient pressure, and the spin susceptibility vanishes at low temperature at 2.1 GPa. Moreover, from the temperature dependence of T_1^{-1}, we obtain the relation of $T_1^{-1} \propto T^{3.1}$.

DOI: 10.1103/PhysRevB.82.115114 PACS number(s): 71.28.+d, 74.70.Kn, 76.60.−k

I. INTRODUCTION

Recently, the Dirac electron system, which is suggested in the graphene,[1] was intensively studied.[1–6] Whereas many transport measurements were performed in the graphene, the magnetic measurement is difficult due to its mesoscopic structure. In organic conductors, α-(BEDT-TTF)$_2$I$_3$ under high pressure is a candidate for this exotic electron system. In contrast to graphene, this material can be prepared as a single crystal. Therefore, accurate characterization of the bulk properties could be performed.

The organic conductor, α-(BEDT-TTF)$_2$I$_3$, in which the conducting layers of the BEDT-TTF (bis-ethylenedithio-tetrathiafulvalene) molecule and the insulating layers of I_3^{-1} alternatively stack along the crystalline c^* axis, forms a two-dimensional electronic system shown in Fig. 1(a).[7] The charge-ordered (CO) state in this salt is theoretically predicted in the consideration of off-site Coulomb repulsion; the CO state is experimentally confirmed by charge disproportionation and the insulating behavior with a spin-singlet state below 135 K.[8–13] It is confirmed that the pattern in the CO state is a horizontal stripe along b axis and the degree of the charge disproportionation is determined in x-ray diffraction (XRD) ($\Delta\rho$=0.5e),[12] vibrational spectroscopy ($\Delta\rho$=0.6e),[9,10] and nuclear-magnetic resonance (NMR) ($\Delta\rho$=0.55e).[13] Moreover, in uniaxial pressure along the a axis, the superconductivity was observed and the relationship between charge fluctuation and the superconductivity was suggested.[14,15]

In hydrostatic pressure above 2.0 GPa, the suppression of the metal-insulator transition and almost-temperature-independent behavior of electrical resistance were observed. In addition, the strong temperature dependence of the Hall coefficient is reported and the high mobility state in low temperature was predicted.[16] The narrow energy gap electron system was suggested by the band calculation of this salt and the zero-gap-semiconductor (ZGS) phase in the noninsulating state is proposed.[17] The band structure of the salt has a discriminative feature. The contact points of the band dispersion are symmetrically located in **k** space and the shapes of the band around the contact points have a titled corn structure and an anisotropic linear dispersion structure.[17] The band structure with linear dispersion is described by the Dirac electron system as similar to graphene,[1–4] inspiring many theoretical and experimental studies.[1–4,17–20]

From this exotic electronic system, non-Pauli-type magnetism is expected. Moreover, Landau level does not form with the magnetic field parallel to conducting plane. Therefore we can obtain the information about magnetic property directly related with band structure in this condition. The spin susceptibility provides the important information of the conducting electron.

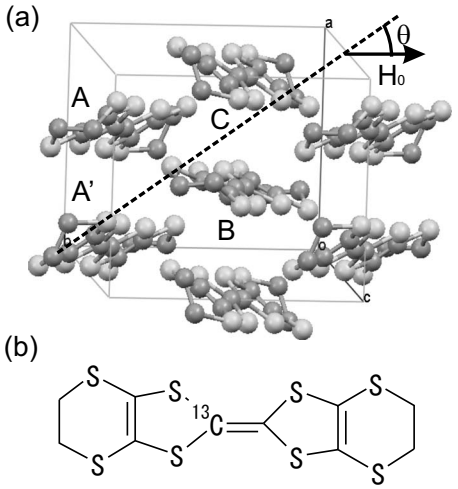

FIG. 1. (a) Projection of the molecular sheet in ab plane of α-(BEDT-TTF)$_2$I$_3$ (Ref. 7). An arrow represents the direction of the magnetic field, which is characterized by θ. (b) Single carbon ^{13}C-enriched BEDT-TTF molecule.

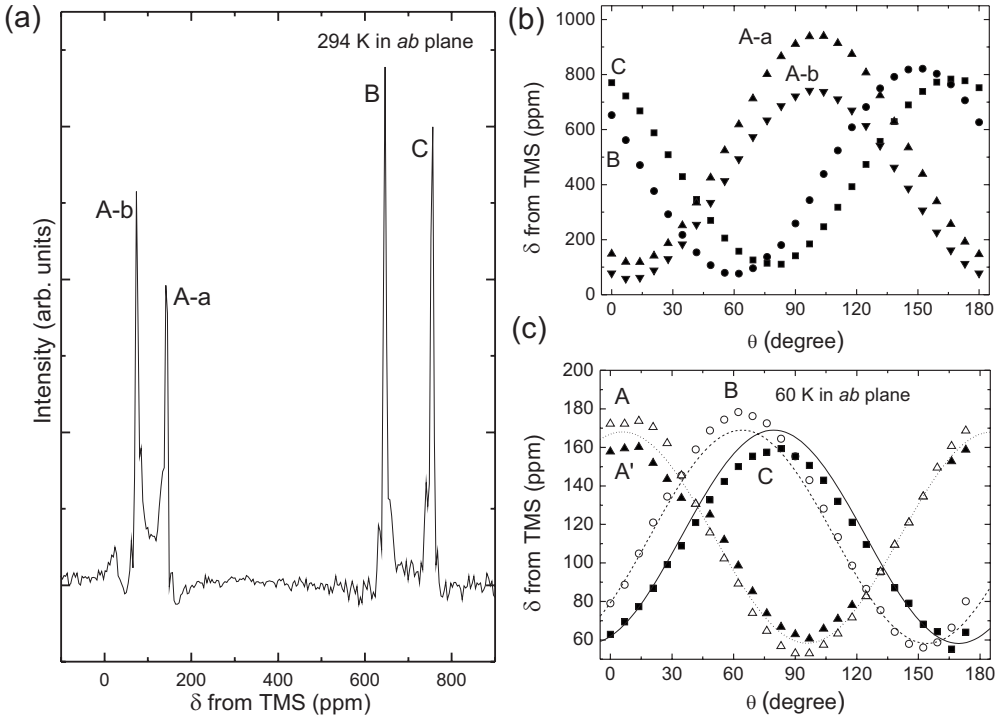

FIG. 2. (a) NMR spectrum at room temperature at an angle of 0° in Fig. 2(b). A-a, A-b, B, and C represent the local atomic sites in α-(BEDT-TTF)$_2$I$_3$. (b) Angular dependence of NMR shift at atomic sites A-a, A-b, B, and C at room temperature (Ref. 13). The angle of θ corresponds to that in Fig. 1(a). (c) Angular dependence of chemical shift in the *ab* plane (Ref. 13). The symbols represent the chemical shift in CO state and the lines represent the chemical shift in ρ=+0.5e. A, A′, B, and C represent the molecular site shown in Fig. 1(a). The angle of θ corresponds to that in Fig. 1(a).

In theoretical study, the spin susceptibility and the spin-lattice relaxation rate at low temperature are expected to be proportional to T and T^3, respectively, which are characterized by the density of state. The spin susceptibility and the spin-lattice relaxation rate depend on the electronic states in the wave number of Fermi energy and the density of state in each molecular site is expected to be different.[21] Since there are three crystallographically independent BEDT-TTF molecules, A, B, and C, in unit cell, a disproportionation between molecular sites is expected. They also predicted the disproportionation of $\chi_C > \chi_A > \chi_B$.

However, the small magnetization from the conducting electron complicates the measurement under pressure due to the background signal from the pressure cell. Due to this difficulty, the spin susceptibility under pressure has not been measured. Moreover, it is difficult to distinguish between three molecular sites, A, B, and C, using static magnetization measurement. NMR, however, can probe the local spin susceptibility at the specific atomic site as a Knight shift and is performed under pressure without the background signal from the pressure cell. In addition, the spin excitation can be detected as the spin-lattice relaxation time, T_1. Therefore, we utilized ^{13}C-NMR to explore the magnetic properties at each molecular site in the ZGS state.

II. EXPERIMENT

A single crystal of α-(BEDT-TTF)$_2$I$_3$ is prepared electrochemically from an isotope-substituted BEDT-TTF molecule and tetra-*n*-butyl-ammonium tri-iodide, [(n-Bu)$_4$N]I$_3$, in benzonitrile. BEDT-TTF, which is substituted by the single side of central C=C bond [Fig. 1(b)], is prepared by the cross coupling between ^{13}C-enriched thioketone and cooled nonenriched ketone. By this method, single side ^{13}C-substituted molecule (larger than 70%), nonsubstituted molecules (26%), and trace amount of double ^{13}C-substituted molecules can be produced.[22] This single side ^{13}C-substituted BEDT-TTF prevents the split of the NMR spectrum caused by the Pake doublet mechanism and simplifies the quantitative analysis of the NMR spectrum and the site assignment. The high-pressure experiment was performed under 2.1 GPa with a NiCrAl clamp cell and Daphne 7373 oil was used as the pressure medium and the internal standard for the NMR shift. The NMR spectra were obtained by fast Fourier transformation of the spin-echo signal with $\pi/2$-π pulse sequence and the spin-lattice relaxation time was determined by the saturation recovery method.

III. RESULT AND DISCUSSION

A. NMR spectrum at room temperature

Figure 2(a) shows NMR spectrum at 294 K and ambient pressure. Due to the symmetry of the crystal, there are two crystallographically independent ^{13}C positions on molecular site A. Therefore, four signals from sites A-a, A-b, B, and C are observed in the paramagnetic state. Only four peaks with the simple sinusoidal curve were observed and the additional

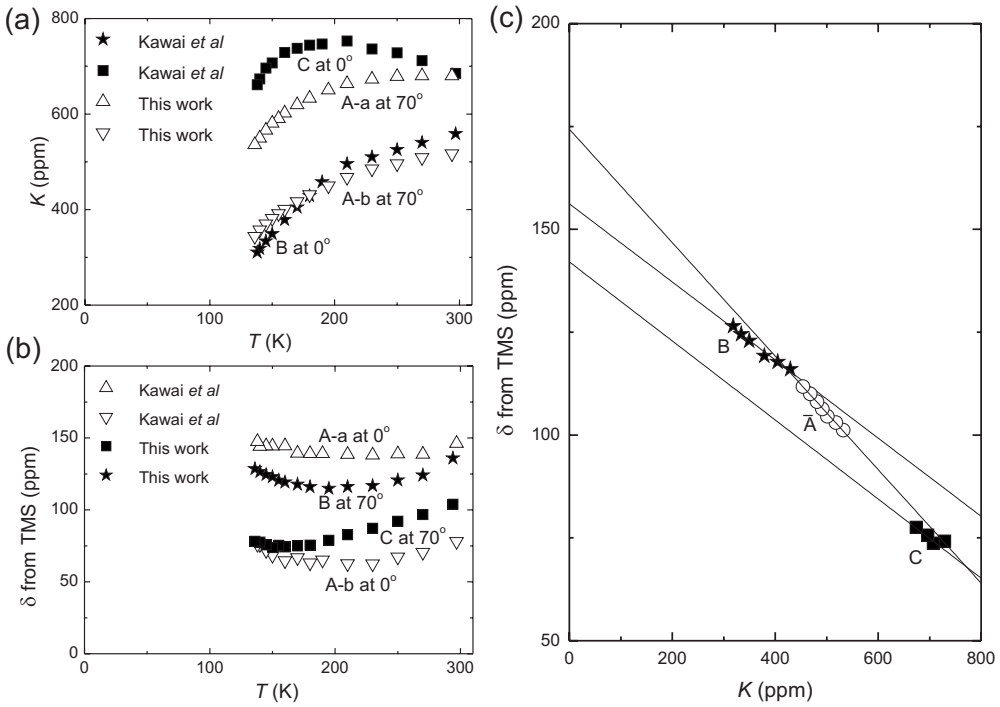

FIG. 3. (a) Knight shift at atomic sites A-a, A-b at 70°, B and C at 0° [filled symbols: previous work (Ref. 13), open symbols: this work]. (b) NMR shift at atomic sites A-a, A-b at 0°, B and C at 70° [filled symbols: this work, open symbols: previous work (Ref. 13)]. (c) δ-K plot at sites $\bar{A}$, B, and C. $\bar{A}$ represents the mean value of the atomic sites A-a and A-b.

eight signals with modulated sinusoidal curve from Pake doublet on $^{13}C{=}{=}^{13}C$ molecule were not observed. That is, the ratio of $^{13}C{=}{=}^{12}C$ to $^{13}C{=}{=}^{13}C$ is much higher and the amount of $^{13}C{=}{=}^{13}C$ in the batch is trace level. From the angular dependence of these peaks in Fig. 2(b), we could perform the site assignment.[13]

B. Determination of hyperfine coupling constant

The NMR shift δ can be expressed as the sum of the Knight shift K and the chemical shift σ. The Knight shift can be also expressed as the product of the hyperfine coupling constant a and the spin susceptibility χ and the hyperfine coupling constant depends on the position of the ^{13}C nuclei. This implies that the NMR shift can be expressed as the following equation:

$$\delta = K + \sigma = a\chi + \sigma. \quad (1)$$

To estimate of the spin susceptibility from the Knight shift on each molecular site, the hyperfine coupling constant and the chemical shift are needed.

Figure 2(c) is the angular dependence of the chemical shifts of three independent BEDT-TTF molecules in the CO state in the ab plane.[13] In the CO state, two A sites split into charge-rich (A) and charge-poor (A′) site and molecular site B becomes charge rich and C becomes charge poor. These shifts indicate the inversion symmetry breaking. The angular dependence of sites A and B is shown by the sinusoidal curve with different phases due to molecular orientation. Those of sites A′ and C behave in the same manner. We stress that the difference of the chemical shift between the charge-rich and charge-poor sites on the ab plane is smaller than 20 ppm, even in large charge disproportionation in the CO state $\Delta\rho = +0.6e$.[10] We can approximately use the mean value of the rich and poor sites, shown by the lines in Fig. 2(c). Subtracting the angular dependence of the chemical shift shown in Fig. 2(c) from that of the NMR shift shown in Fig. 2(b), we can evaluate the angular dependence of the Knight shift and the amplitude of the Knight shift at room temperature as $\Delta K_{\bar{A}} = 430$ ppm, $\Delta K_B = 428$ ppm, and $\Delta K_C = 390$ ppm. Here, $\bar{A}$ represents the mean value of the sites A-a and A-b. Since the amplitude of the Knight shift is expected to be proportional to the local spin susceptibility, the ratio of spin susceptibility can be given as χ_A (294 K):χ_B (294 K):χ_C (294 K) $= \Delta K_{\bar{A}}:\Delta K_B:\Delta K_C = 1:0.99:0.91$.

The temperature dependence of the NMR shift was performed by Kawai *et al.*,[13] suggesting that molecular site B became spin poor and molecular site C became spin rich in the paramagnetic state. Addition to that, we also measured the NMR shift at an angle of 70°. Whereas it is suggested that the charge on each molecular site varies above 200 K,[12] the deviations between the NMR shift and the chemical shift on sites A-a, A-b at 70°, B and C at 0° are larger than the uncertainty of the chemical shift (~20 ppm). Therefore we can obtain the Knight shift on sites A-a, A-b at 70°, sites B and C at 0° as shown in Fig. 3(a), subtracting the chemical shift at 0° and 70° from the observed NMR shift.

The ratio of the hyperfine coupling constant at each molecular site is given from the Knight shift and the spin susceptibility as $a_{\bar{A}}:a_B:a_C = K_{\bar{A}}/\chi_A:K_B/\chi_B:K_C/\chi_C$. Here, $K_i (i = \bar{A}, B, C)$ is the Knight shift at room temperature shown in Fig. 3(a). Considering the equation $2\chi_A + \chi_B + \chi_C = \chi_{total}$, we

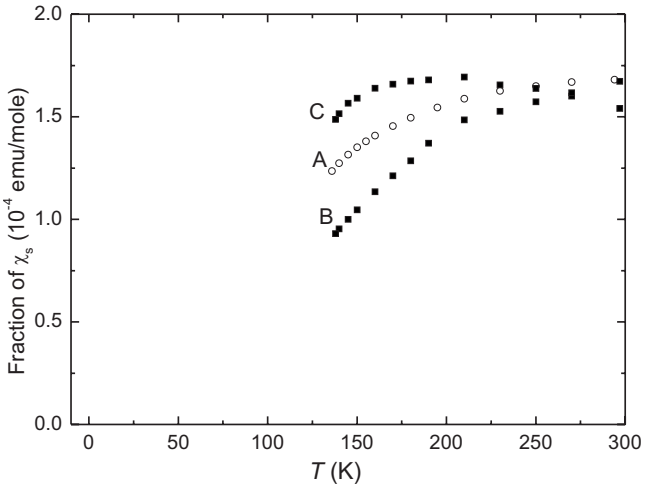

FIG. 4. Fraction of spin susceptibility at molecular sites A, B, and C at ambient pressure.

can determine the hyperfine coupling constants at the three molecular sites as $a_{\bar{A}}$=9.6 kOe/μ_B at 70°, a_B =9.7 kOe/μ_B and a_C=13 kOe/μ_B at 0°.

On the other hand, the NMR shift at each site on another direction is shown in Fig. 3(b). The hyperfine coupling constants at these direction can be evaluated from δ_1-K_2 plots below 150 K shown in Fig. 3(c), in which the chemical shift is almost constant;[12] here, δ_1 is the NMR shift in Fig. 3(b) and K_2 is the Knight shift in Fig. 3(a). NMR shift in Fig. 3(b) can be expressed as

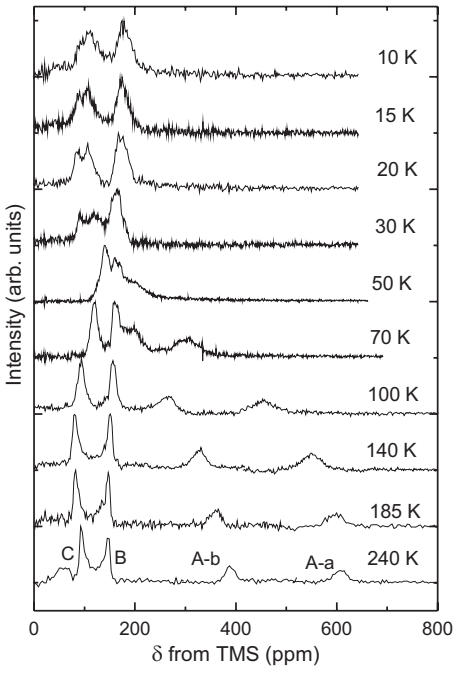

FIG. 5. Temperature dependence of the NMR spectrum at 70° in Fig. 2(b) and at 2.1 GPa. A-a, A-b, B, and C represent the atomic sites corresponding to each peak.

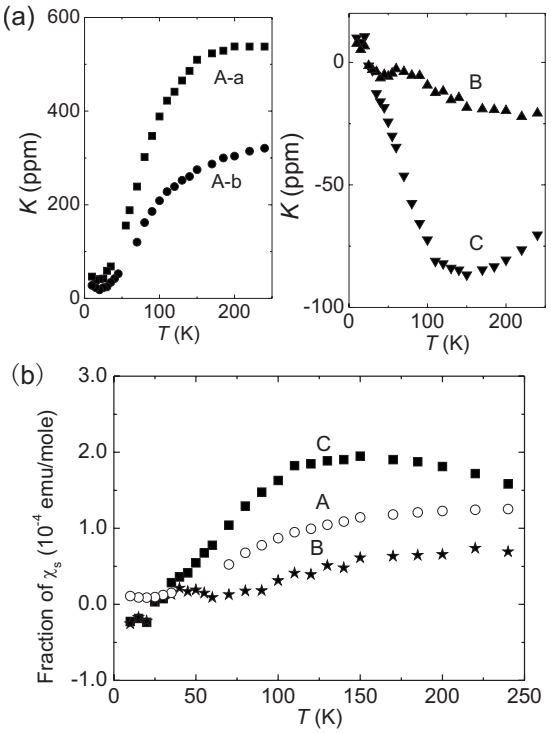

FIG. 6. (a) Knight shift at each atomic site at 70° in Fig. 2(b) and 2.1 GPa. Right figure shows Knight shift at atomic sites A-a and A-b and left figure shows Knight shift at atomic sites B and C. (b) Fraction of spin susceptibility at molecular sites A, B, and C at 2.1 GPa.

$$\delta_1 = \frac{a_1}{a_2} K_2 + \sigma_1. \tag{2}$$

Here, a_1, a_2 and σ_1 are the hyperfine coupling constants and the chemical shift for corresponding field direction. We can deduce a_1 from the slope of δ-K plot and a_2. Thus, we evaluated the hyperfine coupling constants at each molecular site as $a_{\bar{A}}$=−1.2 kOe/μ_B at 0°, a_B=−0.84 kOe/μ_B and a_C= −1.3 kOe/μ_B at 70°, respectively.

C. Spin susceptibility at ambient pressure

Using these hyperfine coupling constants and the Knight shift at the three molecular sites shown in Fig. 3(a), the spin fraction at each molecular site at ambient pressure can be evaluated as shown in Fig. 4. As shown in Fig. 4, the disproportionating behavior of the spin susceptibility was observed. The local spin susceptibility, which is almost same in all the sites at room temperature, steeply decreased at molecular site B and a small pump structure was observed at molecular site C. That is, the disproportionation of the local spin susceptibility between sites B and C developed from room temperature to 140 K. The disproportionation among the three molecular sites is $\chi_C > \chi_A > \chi_B$ at 140 K. The disproportionation of the local spin susceptibility in the paramagnetic state is also observed in α-(BEDT-TTF)$_2$RbHg(SCN)$_4$ and can be thought to be the common nature of α modification.[23] In contrast, XRD suggests that molecular site B became charge rich and molecular

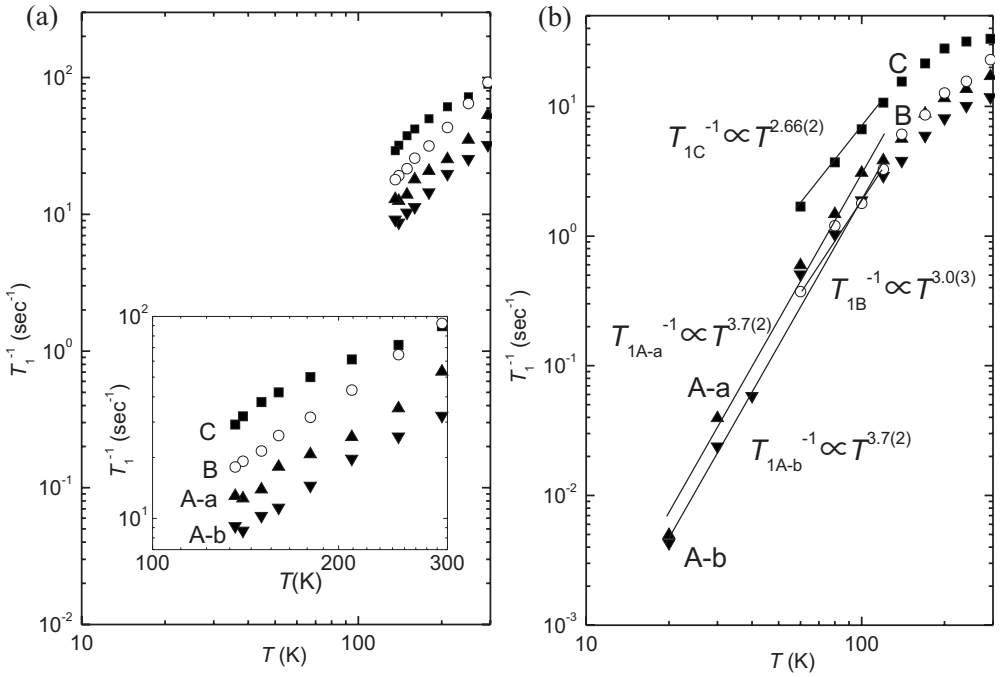

FIG. 7. Temperature dependence of T_1^{-1} at atomic sites A-a, A-b, B, and C in (a) ambient pressure and (b) at 2.1 GPa at 70° in Fig. 2(b). Inset figure shows the extended view. At 2.1 GPa, T_1^{-1} at each atomic site decreases with the relationship of $T_1^{-1} \propto T^{\alpha}$ below 120 K. The relationship of α=3.7(2) at atomic sites A-a and A-b, α=3.0(3) at atomic site B, and α=2.66(2) at atomic site C is represented by solid lines.

site C became charge poor.[12] It is not necessarily the case that the charge on the site is proportional to the spin on the site.[24]

The wave function of the conduction electron with wave number vector $\mathbf{k}$ in α-(BEDT-TTF)$_2$I$_3$ is given as

$$\Psi_{\mathbf{k}} = (c_{\mathbf{k},\mathrm{A}}\phi_{\mathrm{A}} + c_{\mathbf{k},\mathrm{B}}\phi_{\mathrm{B}} + c_{\mathbf{k},\mathrm{C}}\phi_{\mathrm{C}})e^{i\mathbf{k}\cdot\mathbf{r}}. \quad (3)$$

Here, $c_{\mathbf{k},i}$ is linear combination of atomic orbitals coefficient on each site with $\mathbf{k}$ and ϕ_i is highest-occupied molecular orbital function of each site. The charge on each site can be expressed as

$$\rho_{\mathrm{A,B,C}} \propto \sum_{E_{\mathbf{k}}>E_F} |c_{\mathbf{k},\mathrm{A,B,C}}|^2. \quad (4)$$

As the charge on the donor molecule depends on the degree of the hole doping to the neutral molecule, the summation is performed from the hole occupied band over Fermi energy, E_F, in α-(BEDT-TTF)$_2$I$_3$. On the other hand, the local spin susceptibility at each site can be expressed as

$$\chi_{\mathrm{A,B,C}} \propto \sum_{E_{\mathbf{k}}=E_F} |c_{\mathbf{k},\mathrm{A,B,C}}|^2. \quad (5)$$

Only if $c_{\mathbf{k},\mathrm{A,B,C}}$ is independent of $\mathbf{k}$, we can obtain the relationship,

$$\rho_{\mathrm{A,B,C}} \propto \chi_{\mathrm{A,B,C}}. \quad (6)$$

However, our results suggest the wave number dependence of $c_{\mathbf{k},\mathrm{A,B,C}}$ and the relationship between the charge and the spin disproportionation seems to be complicated.

D. Spin susceptibility in ZGS state

The main subject of this research is the behavior of spin susceptibility in the ZGS state. Figure 5 shows the temperature dependence of the NMR spectrum at 70° at 2.1 GPa. Compared with the assignment at ambient pressure, the two peaks at 610 and 410 ppm are assigned as sites A-a and A-b, and the peak at 167 ppm is assigned as site B, and the peak at 120 ppm is assigned as site C. All the peaks shift to the position of the chemical shift shown in Fig. 2(c) at low temperature. These results suggest that the local spin susceptibility vanishes at low temperatures under the ZGS state, whereas Raman-scattering spectroscopy suggests that the degree of charge disproportionation at 2.0 GPa is equal to +0.12e and is almost constant. From the shift of the NMR spectrum in Fig. 5 and our standard of chemical shifts shown in Fig. 2(c), which are 66 ppm for site A and 166 ppm for sites B and C, we can evaluate the Knight shift as shown in Fig. 6(a). For the determination of spin susceptibility, hyperfine coupling constants at an angle of 70° are applicative. Then, we deduced the fraction of spin susceptibility at each molecular sites as shown in Fig. 6(b). The remarkable feature is that the local spin susceptibility at each site rapidly decreases below 120 K and almost vanishes at low temperature; in addition, the degree of disproportionation between the sites at 150 K becomes larger than that at ambient pressure. Especially, the local spin susceptibility at site B is extremely small. In contrast, the degree of charge disproportionation under pressure is almost constant with the temperature in Raman-scattering spectroscopy.[10] In ZGS state, the disproportionation not of charge but of spin contributes to the anomalous physical properties. Conventional metals show the almost-temperature-independent spin sus-

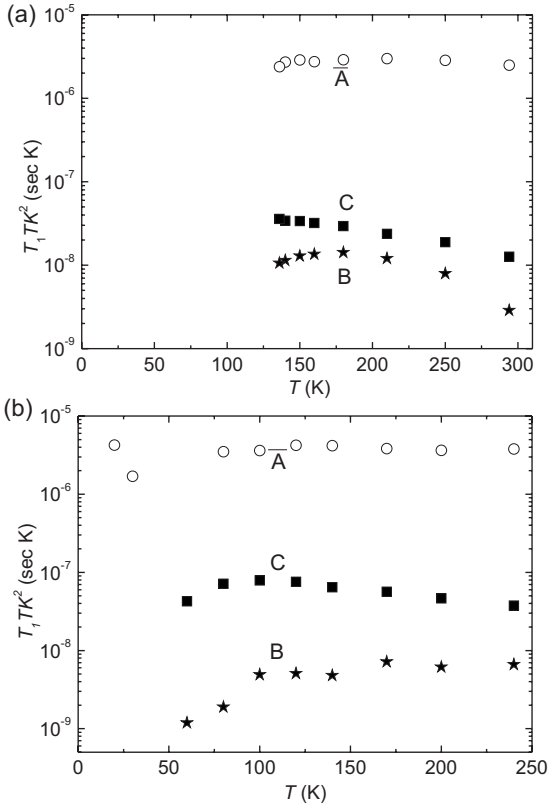

FIG. 8. Temperature dependence of T_1TK^2 at sites Ā, B, and C at (a) ambient pressure and (b) 2.1 GPa at 70° in Fig. 2(b). Ā represents the mean value of atomic sites A-a and A-b.

ceptibility, characterized by the density of state at Fermi level. These anomalous behaviors could be examined by the distinguishable band structure in this salt, for example, the point node structure. The temperature dependence of the carrier density, n, showed T^2 dependence below 100 K from Hall-effect measurement,[16] and this behavior is thought to be related with the decrease in the spin susceptibility in low temperature. In the theoretical study, the disproportionation of the spin fraction between each molecular site is predicted as $\chi_C > \chi_A > \chi_B$ and the spin susceptibility vanishes at low temperature.[21] Our results seem to be consistent with the theoretical prediction.

E. Spin-lattice relaxation time measurement at ambient pressure and high pressure

The characteristic band structure should contribute to the temperature dependence of T_1^{-1}. Figures 7(a) and 7(b) show the temperature dependence of T_1^{-1} around each atomic site at ambient pressure and at 2.1 GPa, respectively. At ambient pressure, T_1^{-1} at B site decreased with decreasing temperature compared with other sites, corresponding to the decrease in the fraction of spin susceptibility. In order to investigate the electric correlation, we show the temperature dependence of T_1TK^2 in Figs. 8(a) and 8(b). The difference of the absolute value of T_1TK^2 at each site is mainly due to the anisotropy of the hyperfine coupling tensor. Whereas T_1TK^2 at site Ā is almost constant, those at sites B and C show the significant temperature dependence at ambient pressure. These behaviors of T_1TK^2 correspond to the disproportionation of the spin density between molecular sites B and C above the CO transition temperature, which is induced by the off-site Coulomb repulsion. At 2.1 GPa and 140 K, the ratio of T_1^{-1} at molecular sites B and C $T_{1,C}^{-1}/T_{1,B}^{-1}=2.6$ is larger than that at ambient pressure. This means that T_1^{-1} at site B decreases as applied the pressure increases and is consistent with the enhancement of the disproportionation observed in the Knight shift.

Figure 8(b) shows the temperature dependence of T_1TK^2 at 2.1 GPa. As same as at ambient pressure, T_1TK^2 at site Ā is almost constant with the comparable magnitude. Above 120 K, the ratio of the spin susceptibility at 2.1 GPa does not show the significant temperature dependence, and T_1TK^2 at sites B and C is also constant, whereas those at ambient pressure show the significant temperature dependence. These results correspond to the temperature independent spin disproportionation at 2.1 GPa. Below 120 K, T_1^{-1} at all the sites decreases steeply, which is the same as the local spin susceptibility, and follows the power law of T, $T_1^{-1} \propto T^{\alpha}$. Using the least-square method against the data below 120 K, we can obtain the relationship that $\alpha=3.7(2)$ at site A-a, $\alpha=3.7(2)$ at site A-b, $\alpha=3.0(3)$ at site B, and $\alpha=2.66(2)$ at site C. The average value of all the sites is related to $\alpha=3.1(2)$. In the case of conventional metals, T_1^{-1} should be followed by $\alpha=1$, so-called Korringa law. The temperature dependence of T_1^{-1} with $\alpha=3$ suggested some node structure in the spin excitation. T_1TK^2 is almost temperature independent, suggesting that the antiferromagnetic contribution with a specific vector is not so strong. In theoretical study the relationship $T_1^{-1} \propto T^3$ is predicted.[21]

IV. CONCLUSION

In summary, in ^{13}C-NMR of α-(BEDT-TTF)$_2$I$_3$ salt at ambient pressure and at 2.1 GPa, we measured the temperature dependence of the NMR spectrum and T_1^{-1}, and examined the analysis of the local spin susceptibility from the NMR shift at each site. The analysis of the spin susceptibility suggested that the degree of spin disproportionation between sites B and C was enhanced in the ZGS state under pressure and the spin susceptibility vanished at low temperature, suggesting the characteristic band dispersion of this salt. The temperature dependence of T_1^{-1} under pressure shows the relation $T_1^{-1} \propto T^{3.1}$; this behavior of T_1^{-1} is indicative of the property of the ZG band structure.

ACKNOWLEDGMENTS

The authors thank T. Kawai of Hokkaido University for the sample preparation. This study was supported in part by a Grant-in-Aid for Science Research (Grant No. 18540306) from the Ministry of Education, Culture, Sports, Science and Technology.

*atkawa@phys.sci.hokudai.ac.jp

[1] K. S. Novoselov, A. K. Geim, S. V. Morozov, D. Jiang, M. I. Katsnelson, I. V. Grigorieva, S. V. Dubonos, and A. A. Firsov, Nature (London) **438**, 197 (2005).
[2] K. S. Novoselov, A. K. Geim, S. V. Morozov, D. Jiang, Y. Zhang, S. V. Dubonos, I. V. Grigorieva, and A. A. Firsov, Science **306**, 666 (2004).
[3] Y. Zhang, Y. W. Tan, H. L. Strormer, and P. Kim, Nature (London) **438**, 201 (2005).
[4] M. I. Katsnelson, K. S. Noveselov, and A. K. Geim, Nat. Phys. **2**, 620 (2006).
[5] F. Wang, Y. Zhang, C. Tian, C. Girit, A. Zettl, M. Crommie, and Y. R. Shen, Science **320**, 206 (2008).
[6] A. B. Kuzmenko, E. van Heumen, F. Carbone, and D. van der Marel, Phys. Rev. Lett. **100**, 117401 (2008).
[7] K. Bender, I. Hennig, D. Schweitzer, K. Dietz, H. Endres, and H. J. Keller, Mol. Cryst. Liq. Cryst. **108**, 359 (1984).
[8] B. Rothaemel, L. Forró, J. R. Cooper, J. S. Schilling, M. Weger, P. Bele, H. Brunner, D. Schweitzer, and H. J. Keller, Phys. Rev. B **34**, 704 (1986).
[9] J. Moldenhauer, Ch. Horn, K. L. Pokhodnia, D. Schweitzer, I. Heinen, and H. J. Keller, Synth. Met. **60**, 31 (1993).
[10] R. Wojciechowski, K. Yamamoto, K. Yakushi, M. Inokuchi, and A. Kawamoto, Phys. Rev. B **67**, 224105 (2003).
[11] S. Moroto, K. I. Hiraki, Y. Takano, Y. Kubo, T. Takahashi, H. M. Yamamoto, and T. Nakamura, J. Phys. IV **114**, 399 (2004).
[12] T. Kakiuchi, Y. Wakabayashi, H. Sawa, T. Takahashi, and T. Nakamura, J. Phys. Soc. Jpn. **76**, 113702 (2007).
[13] T. Kawai and A. Kawamoto, J. Phys. Soc. Jpn. **78**, 074711 (2009).
[14] J. Merino and R. H. McKenzie, Phys. Rev. Lett. **87**, 237002 (2001).
[15] N. Tajima, A. E. Tajima, M. Tamura, Y. Nishio, and K. Kajita, J. Phys. Soc. Jpn. **71**, 1832 (2002).
[16] N. Tajima, M. Tamura, Y. Nishio, K. Kajita, and Y. Ike, J. Phys. Soc. Jpn. **69**, 543 (2000).
[17] S. Katayama, A. Kobayashi, and Y. Suzumura, J. Phys. Soc. Jpn. **75**, 054705 (2006).
[18] N. Tajima, S. Sugawara, R. Kato, Y. Nishio, and K. Kajita, Phys. Rev. Lett. **102**, 176403 (2009).
[19] S. Katayama, A. Kobayashi, and Y. Suzumura, J. Phys.: Conf. Ser. **132**, 012003 (2008).
[20] A. Kobayashi, S. Katayama, Y. Suzumura, and H. Fukuyama, J. Phys. Soc. Jpn. **76**, 034711 (2007).
[21] A. Kobayashi, S. Katayama, and Y. Suzumura, Sci. Technol. Adv. Mater. **10**, 024309 (2009).
[22] M. Yamashita, A. Kawamoto, and K. Kumagai, Synth. Met. **133-134**, 125 (2003).
[23] T. Kawai and A. Kawamoto, Phys. Rev. B **78**, 165119 (2008).
[24] S. Hirose, A. Kawamoto, N. Matsunaga, K. Nomura, K. Yamamoto, and K. Yakushi, Phys. Rev. B **81**, 205107 (2010).